J Biomol NMR (2013) 55:1–9
DOI 10.1007/s10858-012-9691-9

COMMUNICATION

Structural characterization of supramolecular assemblies by ^{13}C spin dilution and 3D solid-state NMR

Birgit Habenstein · Antoine Loquet · Karin Giller · Stefan Becker · Adam Lange

Received: 23 October 2012 / Accepted: 24 November 2012 / Published online: 1 December 2012

Abstract ^{13}C spin diluted protein samples can be produced using [1-^{13}C] and [2-^{13}C]-glucose (Glc) carbon sources in the bacterial growth medium. The ^{13}C spin dilution results in favorable ^{13}C spectral resolution and polarization transfer behavior. We recently reported the combined use of [1-^{13}C]- and [2-^{13}C]-Glc labeling to facilitate the structural analysis of insoluble and non-crystalline biological systems by solid-state NMR (ssNMR), including sequential assignment, detection of long-range contacts and structure determination of macromolecular assemblies. In solution NMR the beneficial properties of sparsely labeled samples using [2-^{13}C]-glycerol (^{13}C labeled Cα sites on a ^{12}C diluted background) have recently been exploited to provide a bi-directional assignment method (Takeuchi et al. in J Biomol NMR 49(1):17–26, 2011). Inspired by this approach and our own recent results using [2-^{13}C]-Glc as carbon sources for the simplification of ssNMR spectra, we present a strategy for a bi-directional sequential assignment of solid-state NMR resonances and additionally the detection of long-range contacts using the combination of ^{13}C spin dilution and 3D NMR spectroscopy. We illustrate our results with the sequential assignment and the collection of distance restraints on an insoluble and non-crystalline supramolecular assembly, the *Salmonella typhimurium* type III secretion system needle.

Keywords Solid-state NMR · Isotopic labeling · Resonance assignment · Structure determination · Secretion systems · Supramolecular assemblies

Introduction

3D structure determination by solution nuclear magnetic resonance (NMR) spectroscopy relies on the unambiguous and reliable assignment of the NMR signals and the detection of long-range distance restraints (Wüthrich 1986; Guntert 1998; Ferentz and Wagner 2000; Markwick et al. 2008; Banci et al. 2010). However, solution NMR techniques are limited to protein states with sufficiently short correlation times τ_c, which is not the case for a broad range of biological systems. This includes high-molecular weight protein assemblies, fibrils, aggregates and membrane proteins in a native-like lipid environment that can be readily studied by solid-state NMR (ssNMR) [for reviews see (Griffin 1998; Tycko 2006; McDermott and Polenova 2007; Renault et al. 2010; Hong et al. 2012b; Sun et al. 2012; Reif 2012)]. Recent progress in high-resolution ssNMR has allowed investigating protein assemblies and membrane protein structures of growing complexity (Petkova et al. 2002; Wasmer et al. 2008; Helmus et al. 2008; Nielsen et al. 2009; Schneider et al. 2010; Jehle et al. 2010; Barbet-Massin et al. 2010; Ader et al. 2010; Hu et al. 2010; Lewandowski et al. 2011; Ward et al. 2011; Bertini et al. 2011; Comellas et al. 2012; Hong et al. 2012a, b; Lopez del Amo et al. 2012; Eddy et al. 2012; Loquet et al. 2012b; Habenstein et al. 2012). Yet, the assignment of the ssNMR signals remains error-prone, labour-consuming and a major experimental time investment. Sequential assignment strategies in ssNMR are based on the combination of

Electronic supplementary material The online version of this article (doi:10.1007/s10858-012-9691-9) contains supplementary material, which is available to authorized users.

B. Habenstein · A. Loquet · K. Giller · S. Becker · A. Lange (✉)
Department of NMR-based Structural Biology, Max Planck Institute for Biophysical Chemistry, Am Fassberg 11, 37077 Göttingen, Germany
e-mail: adla@nmr.mpibpc.mpg.de

several two-dimensional (2D) spectra. For more complex systems three-dimensional (3D) spectroscopic techniques are increasingly applied to alleviate the spectral overlap, enabling assignment of proteins up to 33 kDa (Habenstein et al. 2011). The spectroscopic features of ^{13}C spin diluted protein samples, based on sparsely labeled glucose or glycerol (LeMaster and Kushlan 1996; Hong 1999; Castellani et al. 2002; Teilum et al. 2006; Lundstrom et al. 2007; Higman et al. 2009; Loquet et al. 2010, 2011, 2012b), provide an additional tool to access more complicated biomolecules. In solution NMR, favorable spectroscopic properties of sparsely labeled samples using [2-^{13}C]-glycerol (^{13}C labeled Cα sites on a ^{12}C diluted background) have recently been used by the Wagner's group (Takeuchi et al. 2011) to establish a bi-directional assignment strategy. In line with this approach and our experience on proteins labeled with [2-^{13}C]glucose carbon sources (Loquet et al. 2010, 2011, 2012b; Lv et al. 2012), we propose a simple strategy for ssNMR resonance assignment using a combination of ^{13}C spin dilution and 3D NMR spectroscopy, including only one bi-directional spectrum. Furthermore we show that essentially the same approach, employing longer ^{13}C–^{13}C mixing times, allows for the detection of long-range distance restraints with high sensitivity and resolution.

We demonstrate the applicability of our method on the needle of the *Salmonella typhimurium* type 3 secretion system (T3SS) (Cornelis 2006; Galan and Wolf-Watz 2006; Loquet et al. 2012a), a complex nanomachine involved in bacterial infection. The needle consists of multiple copies of a single protein subunit (protein PrgI, 8.8 kDa), assembled into a filamentous suprastructure. The atomic structure of the T3SS needle was recently solved in our laboratory (Loquet et al. 2012b) on the basis of ssNMR distance restraints.

Materials and methods

Sample preparation

We overexpressed, purified and polymerized the *S. typhimurium* PrgI protein as described in ref (Loquet et al. 2012b). The PrgI needle filaments (corresponding approximately to 10 mg of material) were packed into a 3.2 mm solid-state NMR rotor. 4,4-dimethyl-4-silapentane-1-sulphonic acid (DSS) was added as an internal reference for chemical shift and sample temperature referencing.

NMR spectroscopy

Solid-state NMR spectra were recorded on a 20 T wide-bore spectrometer (Bruker Biospin, Germany), equipped with a triple-resonance 3.2 mm MAS probe. A spinning rate of 11 kHz was used at a sample temperature around 7 °C (280 K). Chemical shifts were calibrated with DSS as internal reference. ^{1}H–^{15}N transfer was achieved by a ramped cross-polarization (CP) of 1750 μs, and ^{15}N–^{13}C transfer by a SPECIFIC CP (Baldus et al. 1998) step of 7 ms using a tangential ramp on ^{13}C. PDSD (Bloembergen 1949) was used for the ^{13}C–^{13}C transfer with mixing times as indicated in the main text. ^{1}H decoupling with an r.f. field strength of 83 kHz was applied during the ^{15}N–^{13}C transfer (CW) and acquisition times [SPINAL-64 (Fung et al. 2000)], and scalar ^{13}C–^{15}N couplings were refocused with a 180° pulse on ^{13}C during the ^{15}N evolution period or by WALTZ decoupling during ^{13}C evolution periods (Shaka et al. 1983). Maximum acquisition times were 5 ms for the indirect dimensions and 15 ms for the direct dimension, leading to a total experimental time of 10 and 13 days for the spectra with 250 and 850 ms mixing time, respectively. All NMR spectra were processed with NMRpipe7 (Delaglio et al. 1995).

Assignment analysis

All NMR spectra were analyzed using CcpNmr (Vranken et al. 2005).

Results

Our method combines 3D ssNMR techniques and the spectroscopic features of ^{13}C spin diluted protein samples. The use of protein samples, isotopically labeled using [2-^{13}C]-glucose (Glc) as sole carbon source, provides a reduced number of ^{13}C labeled carbon sites (Hong 1999; Teilum et al. 2006; Lundstrom et al. 2007). This engenders an improved spectral resolution by removing the majority of one-bond J- and dipolar ^{13}C–^{13}C couplings [an improvement in linewidth by a factor of ∼2 as measured on the T3SS needle protein PrgI for the ^{13}C dimension (Loquet et al. 2011)] and an increased sensitivity in 2D proton-driven spin diffusion [PDSD (Bloembergen 1949)] spectra that results from enhanced polarization transfer due to the very sparse ^{13}C labeling, reducing the number of possible polarization pathways and therefore increasing the cross-peak signal-to-noise (Loquet et al. 2010). Notably, ^{13}C spin dilution based on [2-^{13}C]-Glc as the sole carbon source during protein expression introduces ^{13}C labeling in all Cα positions except for leucines and no simultaneous Cα/Cβ labeling except for valines and isoleucines. The improved linewidth and enhanced polarization transfer efficiency compensates the loss of sensitivity due to the sparse ^{13}C occurrence (max. labeling efficiency of 50 % for Cα). The ^{13}C labeling pattern and the good sequential

$^{13}C\alpha$–$^{13}C\alpha$ polarization transfer in PDSD-type experiments suggests the implementation of a straightforward 3D $N_iC\alpha_iCX_{i\pm n}$ experiment (Supporting Information, Figure S1), where the N_i–$C\alpha_i$ pair provides a starting point for the assignment and the $C\alpha_i$–$CX_{i\pm n}$ transfer establishes sequential and long-range contacts. The experiment consists of an initial ^{15}N–$^{13}C\alpha$ step followed by a PDSD mixing period. The length of the mixing period will determine the extent of signals encoding for sequential, medium or long-range distance restraints visible in the 3D spectrum.

First, in order to address the sequential assignment of the NMR resonances of the T3SS needle protein PrgI, the 3D experiment is implemented with maximal sequential $C\alpha_i$–$C\alpha_{i\pm1}$ polarization transfer, achieved using a short PDSD mixing period (250 ms). The preceding ^{15}N–$^{13}C\alpha$ step is optimized for a maximal polarization transfer to $C\alpha$ (i.e. SPECIFIC N_i–$C\alpha_i$) (Baldus et al. 1998) and the polarization then further diffuses to the neighboring $C\alpha$s and establishes bi-directional sequential i to $i \pm 1$ connectivities (Fig. 1a), reminiscent of the above discussed solution NMR approach (Takeuchi et al. 2011). The proposed method, implemented in a 3D fashion, takes advantage of the good polarization transfer, similar to a previous approach proposed by Oschkinat and coworkers to facilitate the identification of ssNMR signals of selectively glycerol labeled proteins (Castellani et al. 2003; Higman et al. 2009). Our approach benefits from a higher spin dilution (one carbon labeled out of 6), leading to favourable spectroscopic features as described in details in (Loquet et al. 2011) that make the implementation of a bi-directional spectrum possible. The approach allows for a rapid and simple analysis of the 3D NCC spectrum, where the resonance peaks can sequentially be assigned following the scheme shown in Fig. 1b. The ^{15}N plane of the residue i ^{15}N resonance frequency is plotted in the middle of the assignment scheme. From the intraresidue $N_iC\alpha_iC\alpha_i$ correlation peak on the diagonal (black) two pathways are discernible at the $C\alpha$ resonance frequency of residue i: one towards the $i - 1$ residue ($N_iC\alpha_iC\alpha_{i-1}$ correlation peak in blue) and one towards the $i + 1$ residue ($N_iC\alpha_iC\alpha_{i+1}$ correlation peak in pink). In the ^{15}N plane of the following (or preceding) residue, three correlation peaks again reveal the intraresidue $N_{i+1}C\alpha_{i+1}C\alpha_{i+1}$ correlation (or

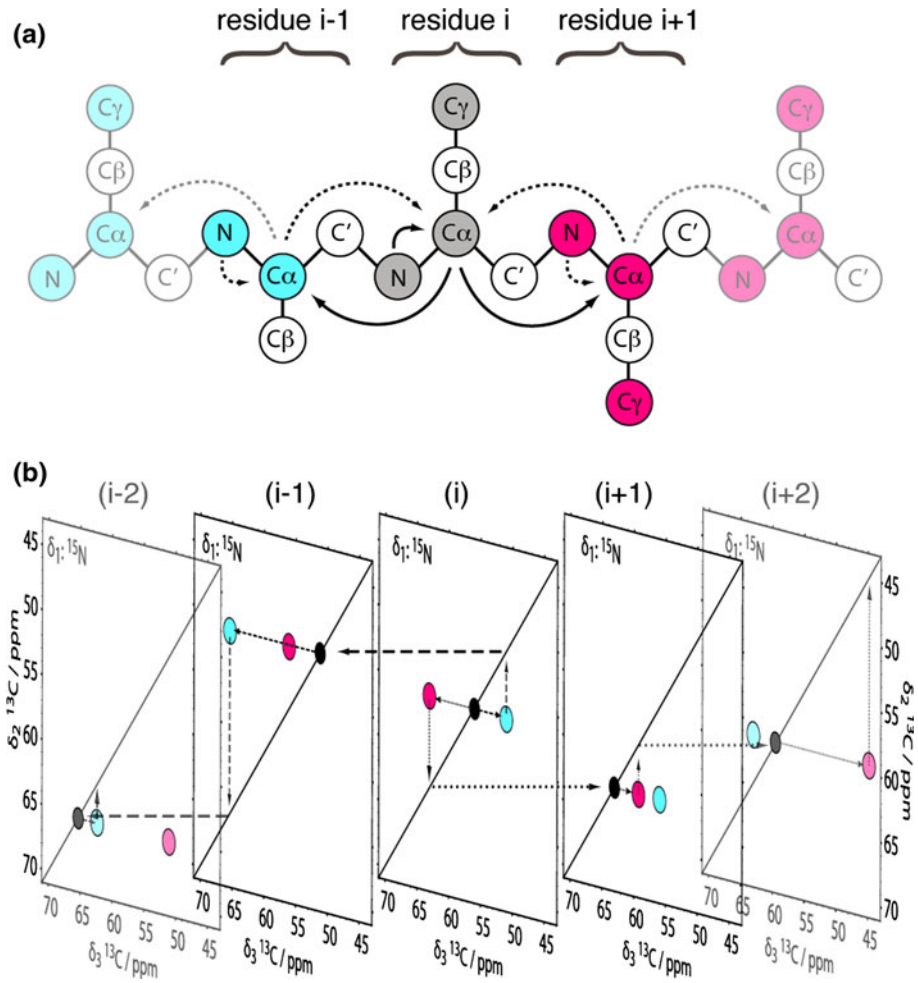

Fig. 1 Solid-state NMR sequential resonance assignment via a bi-directional 3D NCαCX experiment. **a** Scheme of the polarization transfer pathway in a [2-^{13}C]-Glc labelled peptide. From the nitrogen of residue i (N_i; *grey*) the magnetization is transferred to $C\alpha_i$ and then further to $C\alpha_{i+1}$ (*pink*) and $C\alpha_{i-1}$ (*blue*); **b** Sequential walk starting from the ^{15}N (middle ^{15}N plane) and $C\alpha$ resonance frequencies of residue i (*black circle*) towards $C\alpha_{i+1}$ (*pink*) and $C\alpha_{i-1}$ (*blue*)

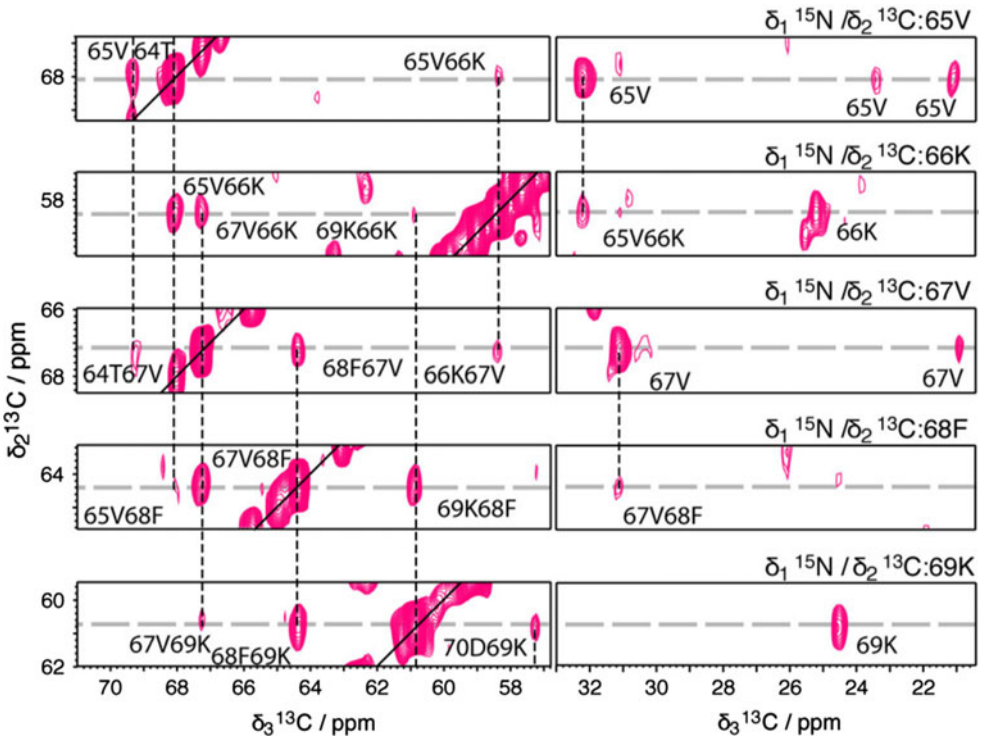

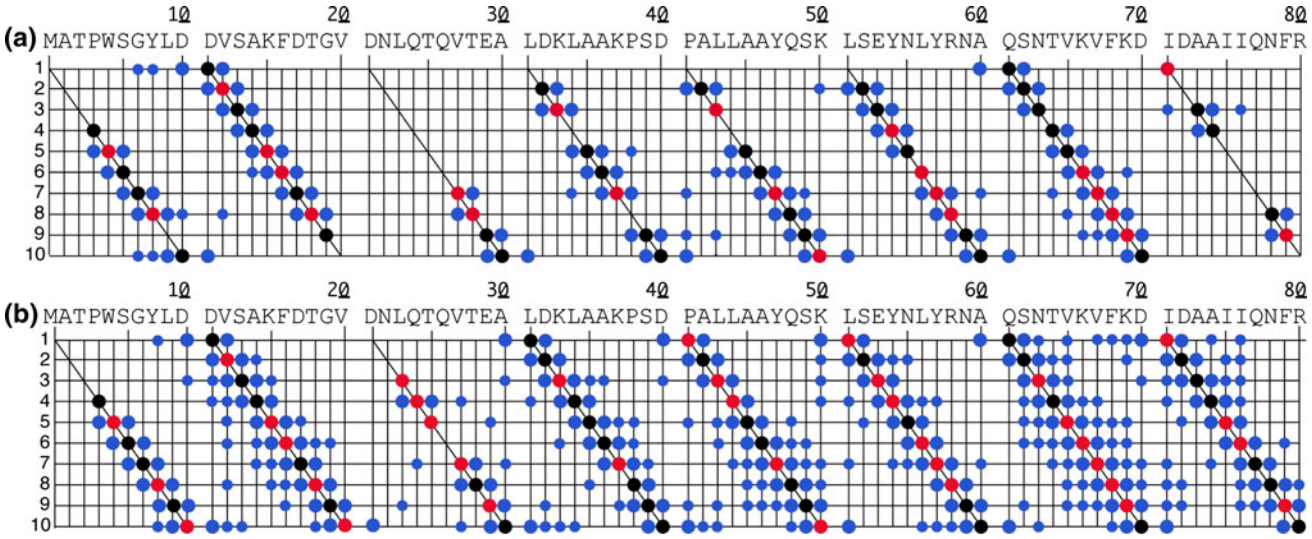

Fig. 2 3D assignment of the stretch Val65 to Lys69 of the *S. typhimurium* type 3 secretion system needle protein PrgI; shown with 2D ^{13}C–^{13}C planes extracted from the 3D NCαCX ($\tau_{mix} = 250$ ms)

Fig. 3 Sequential assignment of the *S. typhimurium* type 3 secretion system needle. Assignment of sequential and medium range ($i - j \leq 4$) contacts in a 3D NCαCX spectrum, with **a** $\tau_{mix} = 250$ ms and **b** $\tau_{mix} = 850$ ms. The primary sequence is plotted above the connectivity plot in which *filled circles* indicate the observed correlations in blocks of 10 residues. The *colour scheme* indicates the different types of observed correlations: $N_iC\alpha_iC\alpha_i$ *black*; $N_iC\alpha_iCX_i$ *red*; $N_iC\alpha_iCX_{i\pm n}$ *blue* (*big circles* for sequential $N_iC\alpha_iCX_{i\pm1}$ correlations)

$N_{i-1}C\alpha_{i-1}C\alpha_{i-1}$), the connection to residue i, $N_{i+1}C\alpha_{i+1}C\alpha_i$ (or $N_{i-1}C\alpha_{i-1}C\alpha_i$), as well as to the next neighbor ($i \pm 2$), $N_{i+1}C\alpha_{i+1}C\alpha_{i+2}$ (or $N_{i-1}C\alpha_{i-1}C\alpha_{i-2}$). The described approach allows for the navigation through the 2D NCα planes of one 3D spectrum using two constant frequencies (e.g. of $C\alpha_i$ and $C\alpha_{i+1}$) throughout each step of the sequential walk (a requirement for the unambiguous sequential assignment). Other 3D methods, based on the use of uniformly labeled samples, usually involve the recording of several 3D spectra (Pauli et al. 2001; Shi et al. 2009; Sperling et al. 2010; Schuetz et al. 2010; Habenstein et al. 2011): one for the spin system identification ($N_iC\alpha_iC\beta_i$, $N_iC\alpha_iCX_i$, $N_i(C\alpha_i)C\beta_iCX_i$), one to establish the sequential connectivity to the residue $i - 1$ ($C\alpha_iN_iCO_{i-1}$,

$C\alpha_iN_i(CO_{i-1})C\alpha_{i-1}$, $C\alpha_iN_i(CO_{i-1})CX_{i-1}$) and one to identify the spin system of residue $i-1$ ($N_iCO_{i-1}C\alpha_{i-1}$, $N_iCO_{i-1}CX_{i-1}$, $N_i(CO_{i-1})C\alpha_{i-1}C\beta_{i-1}$). In contrast, our approach allows for a bi-directional sequential assignment using a single spectrum.

Figure 2 shows 2D ^{15}N–^{13}C strips of a 3D NCαCX spectrum (PDSD mixing time: 250 ms) recorded on [2-^{13}C]-Glc labeled T3SS PrgI needles (sequential walk for the stretch Val65 to Lys69). Despite the small spectral dispersion (PrgI is a predominantly α-helical protein (Loquet et al. 2012b)) and the high abundance of Leu for which Cα is not labeled (10 % of all residues) we achieved an 80 % complete ab initio sequential assignment using only the 3D and a previously recorded 2D ^{13}C–^{13}C PDSD spectrum [20 ms mixing to detect intra-residue connections as described in (Loquet et al. 2011)]. Figure 3a summarizes all connectivities that have been used throughout the sequential assignment. The [2-^{13}C]-Glc sparse labeling has the additional advantage to provide a characteristic ^{13}C pattern for aromatic residues. Cα and Cγ are labeled (Cβ and Cδ are unlabeled which results in enhanced $^{13}C\alpha$–$^{13}C\gamma$ polarization transfer), leading to very intense $N_iC\alpha_iC\gamma_i$ cross-peaks (Fig. 4a). A rapid and unambiguous identification of the aromatic residues, including their ^{15}N resonance frequency (see Fig. 4b) is therefore straightforward. The sequential assignment is also facilitated by the occurrence of side-chain interresidue cross-peaks ($N_iC\alpha_iCX_{i\pm n}$) in addition to the $N_iC\alpha_iC\alpha_{i\pm n}$ correlations

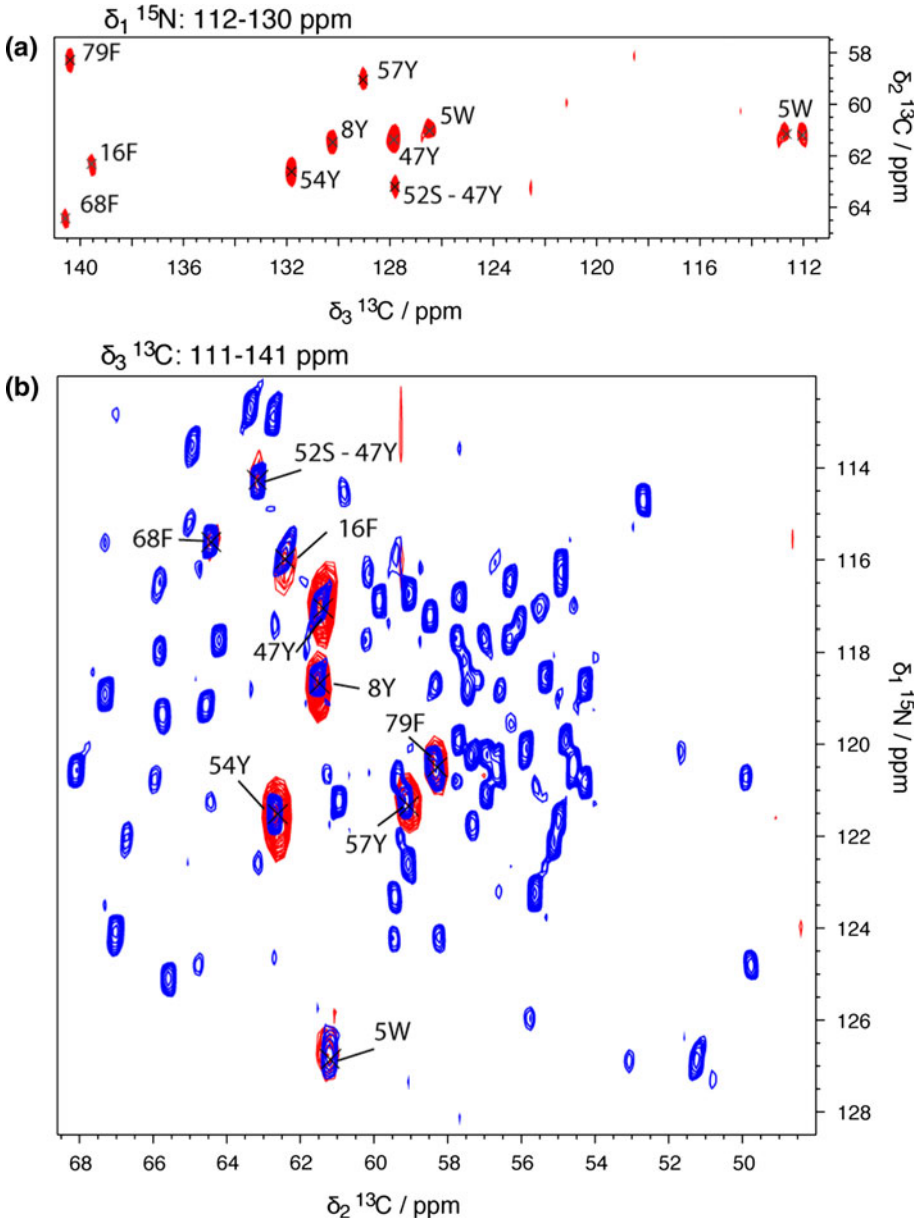

Fig. 4 Aromatic region of 3D NCaCX spectrum ($\tau_{mix} = 250$ ms) of T3SS PrgI needles (*red*). Projections of the spectrum **a** onto the ^{15}N dimension (112–130 ppm) and **b** onto the aromatic region in the direct dimension (^{13}C, 111–141 ppm), superimposed with a 2D NCa spectrum in *blue*

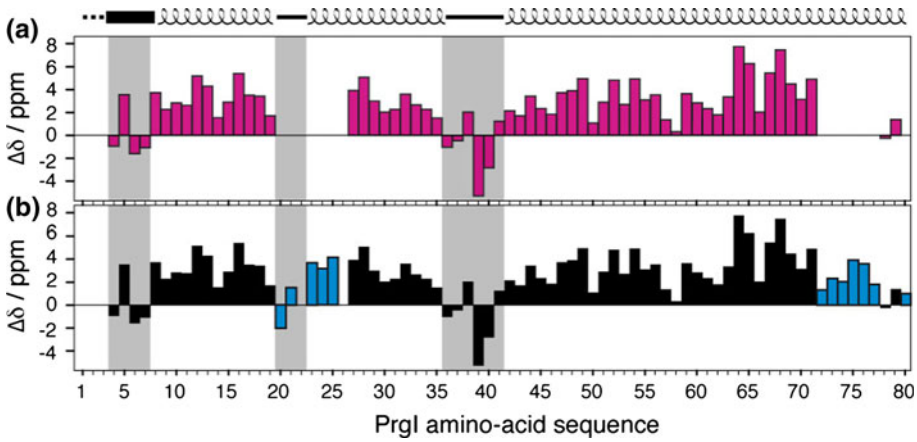

Fig. 5 **a** Secondary structure of the *S. typhimurium* type 3 secretion system needle PrgI extracted from the analysis of a single 3D NCαCX spectrum (τ_{mix} = 250 ms), positive ΔδCα values indicate α-helical structure; **b** complementary secondary structure information from the 3D NCαCX spectrum with long mixing time (τ_{mix} = 850 ms; *blue*)

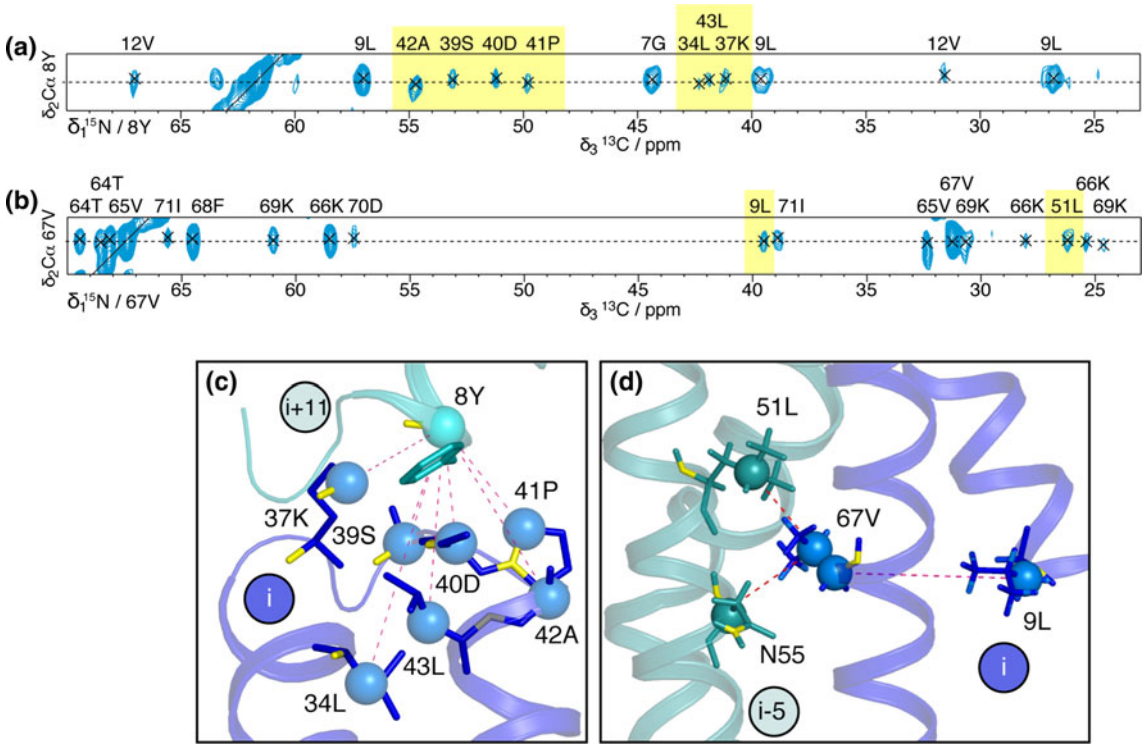

Fig. 6 Collection of long-range solid-state NMR distance restraints. Restraints collected for Tyr8 (**a**) and Val67 (**b**), using the 3D NCαCX spectrum with long mixing time (τ_{mix} = 850 ms); shown are 2D ^{13}Cα–^{13}CX planes. Long-range restraints are *highlighted* in *yellow*. The restraints are shown on the solid-state NMR atomic model of the type 3 secretion system needle [PDB entry 2LPZ, (Loquet et al. 2012b)], for Tyr8 (**c**) and Val67 (**d**)

(Fig. 2). At this stage, a unique 3D NCαCX spectrum has allowed for the identification and confirmation of the global secondary structure of the T3SS needle assembly (see Fig. 5a). We note that our approach could push the limits of reliable sequential assignments to higher protein molecular weights, as the ^{13}C spin dilution decreases the spectral crowding in 3D experiments through the improvement of resolution and the reduced number of observable ^{13}C resonances. For biological systems that exhibit moderate to low spectral resolution, such as several reported amyloid fibrils (Tycko 2006), the improvement of resolution mostly corresponding to the removal of one-bond ^{13}C–^{13}C J-couplings will become negligible, while spectral crowding will still be reduced due to the sparse ^{13}C labeling and an additional dimension.

The collection of ^{1}H–^{1}H–NOE-based distance restraints is the basis for structural investigations by solution NMR (Wüthrich 1986). In ssNMR dipolar truncation effects,

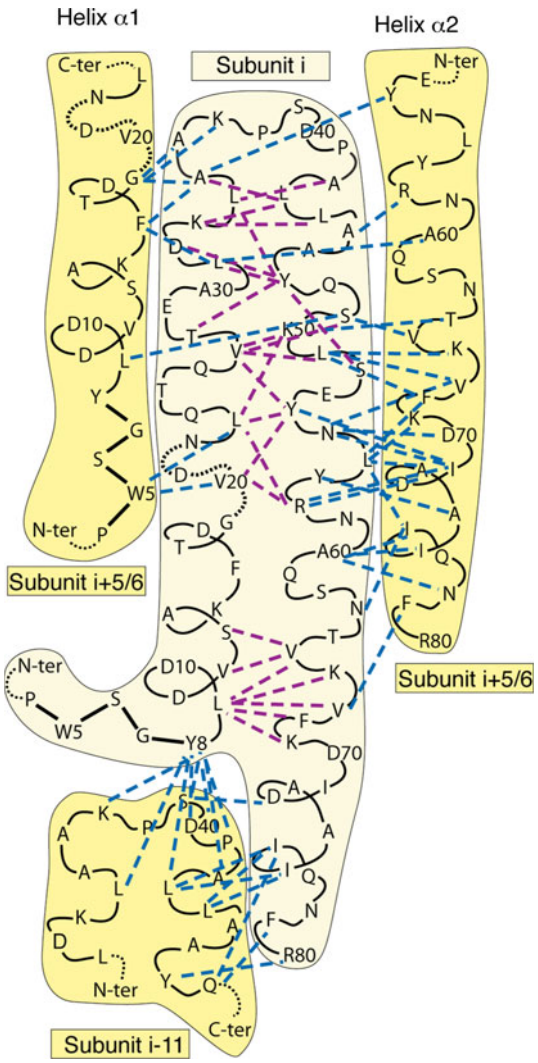

Fig. 7 Summary of the solid-state NMR distance restraints collected on the *S. typhimurium* type 3 secretion system needle PrgI detected in the 3D NCαCX (τ_{mix} = 850 ms) spectrum. *Lines* indicate intrasubunit (*purple*) and intersubunit (*blue*) long-range contacts

present in uniformly ^{13}C labeled proteins, complicate the detection of small dipolar couplings (i.e. long distances) (Hodgkinson and Emsley 1999).

We recently demonstrated the feasibility to detect long-range distances by the use of ^{13}C spin dilution based on [1-^{13}C]- and [2-^{13}C]-Glc (Loquet et al. 2010, 2011) and ultimately to determine high-resolution protein structures (Loquet et al. 2012b), employing 2D ^{13}C–^{13}C experiments. A major issue during the collection of long-range distance restraints is the unambiguous identification (i.e. a unique chemical shift frequency per dimension) of cross-peaks. Here we extend our approach to 3D spectroscopy, in order to reduce the chemical shift degeneracy problem occurring in 2D experiments, by implementing the NCαCX experiment with a long mixing period (t_{mix} = 850 ms, see Supplementary Figure S2 for several ^{15}N planes representing 2D ^{13}Cα–^{13}CX correlations), adequate to detect long-range correlations in 2D (Loquet et al. 2012b).

Figure 3b summarizes the collection of signals that encode for medium-range ($|i - j| \leq 4$) information based on the 850 ms mixing spectrum. We collected 181 medium-range correlations that helped to complete and cross-validate the sequential assignment to a high level (93 % of the ^{13}Cα and ^{15}N atoms). The combination of both 3D spectra permits therefore the near-complete secondary structure analysis (Fig. 5b). In addition to medium-range correlations, we assigned 73 signals encoding for long-range distance restraints. The ambiguity in the assignment of long-range restraints in a 3D spectrum is minimized compared to the assignment in 2D—providing restraints that involve at least one Cα. Figure 6 exemplifies the collection of long-range contacts that are established by the N–Cα pair of residues Tyr8 and Val67, as shown with 2D ^{13}C–^{13}C strips (Fig. 6a, b). Most of the long-range restraints involving these residues correspond to intermolecular (i.e. PrgI subunit–subunit) contacts, as presented in Fig. 6c, d. The 73 long-range restraints include 31 previously unassigned signals compared to the input data used for the structure calculation of the T3SS needle (Loquet et al. 2012b) and will be used to refine the atomic model we have reported. In Fig. 7 all observed long-range signals are presented on the structural model. In 8 cases multiple connections per residue are observed which makes these contacts more reliable (Ala60–Ile76; Tyr8–Ser39; Ala36–Gly19; Ala35–Gly19; Val65–Ser13; Leu56–Lys69; Tyr47–Leu34; Leu56–Ile76). The detected restraints in the 3D experiment yield therefore unambiguous information about the different inter-subunit interfaces in the T3SS needle assembly. The third dimension significantly increases the long-range restraint assignment reliability, leading to additional restraints compared to the previous analysis only based on 2D spectra (Loquet et al. 2012b). The latter result confirms previous ssNMR investigations using [1,3-^{13}C]- or [2-^{13}C]glycerol as carbon source where long-range distances could be obtained for a microcrystalline protein using 3D techniques (Castellani et al. 2003).

The here demonstrated approach is simple and sensitive and therefore likely to be of general use for the rapid assignment of proteins with highly variable molecular weights. It will be a valuable approach to tackle larger filamentous bacterial systems, such as flagellar filaments (Yonekura et al. 2003).

Acknowledgments We thank J.-P. Demers for discussions and B. Angerstein for expert technical assistance. This work was supported by the Max Planck Society, the DFG (Emmy Noether Fellowship to A. Lange), the Fondation Bettencourt Schueller (to A. Loquet), EMBO (Postdoctoral Fellowship to A. Loquet), and the European Union Seventh Framework Program under Grant Agreement 261863 (Bio-NMR).

References

Ader C, Frey S, Maas W, Schmidt HB, Gorlich D, Baldus M (2010) Amyloid-like interactions within nucleoporin FG hydrogels. Proc Natl Acad Sci USA 107(14):6281–6285

Baldus M, Petkova AT, Herzfeld J, Griffin RG (1998) Cross polarization in the tilted frame: assignment and spectral simplification in heteronuclear spin systems. Mol Phys 95:1197–1207

Banci L, Bertini I, Luchinat C, Mori M (2010) NMR in structural proteomics and beyond. Prog Nucl Magn Reson Spectrosc 56(3):247–266

Barbet-Massin E, Ricagno S, Lewandowski JR, Giorgetti S, Bellotti V, Bolognesi M, Emsley L, Pintacuda G (2010) Fibrillar vs crystalline full-length beta-2-microglobulin studied by high-resolution solid-state NMR spectroscopy. J Am Chem Soc 132(16):5556–5557. doi:10.1021/ja1002839

Bertini I, Gonnelli L, Luchinat C, Mao J, Nesi A (2011) A new structural model of Abeta40 fibrils. J Am Chem Soc 133(40):16013–16022

Bloembergen N (1949) On the interaction of nuclear spins in a crystalline lattice. Physica 15:386–426

Castellani F, van Rossum B, Diehl A, Schubert M, Rehbein K, Oschkinat H (2002) Structure of a protein determined by solid-state magic-angle-spinning NMR spectroscopy. Nature 420(6911):98–102

Castellani F, van Rossum BJ, Diehl A, Rehbein K, Oschkinat H (2003) Determination of solid-state NMR structures of proteins by means of three-dimensional 15N–13C-13C dipolar correlation spectroscopy and chemical shift analysis. Biochemistry 42(39):11476–11483

Comellas G, Lemkau LR, Zhou DH, George JM, Rienstra CM (2012) Structural intermediates during alpha-synuclein fibrillogenesis on phospholipid vesicles. J Am Chem Soc 134(11):5090–5099

Cornelis GR (2006) The type III secretion injectisome. Nat Rev Microbiol 4(11):811–825

Delaglio F, Grzesiek S, Vuister GW, Zhu G, Pfeifer J, Bax A (1995) NMRPipe: a multidimensional spectral processing system based on UNIX pipes. J Biomol NMR 6:277–293

Eddy MT, Ong TC, Clark L, Teijido O, van der Wel PC, Garces R, Wagner G, Rostovtseva TK, Griffin RG (2012) Lipid dynamics and protein-lipid interactions in 2D crystals formed with the beta-barrel integral membrane protein VDAC1. J Am Chem Soc 134(14):6375–6387

Ferentz AE, Wagner G (2000) NMR spectroscopy: a multifaceted approach to macromolecular structure. Q Rev Biophys 33(1):29–65

Fung BM, Khitrin AK, Ermolaev K (2000) An improved broadband decoupling sequence for liquid crystals and solids. J Magn Reson 142:97–101

Galan JE, Wolf-Watz H (2006) Protein delivery into eukaryotic cells by type III secretion machines. Nature 444(7119):567–573

Griffin RG (1998) Dipolar recoupling in MAS spectra of biological solids. Nat Struct Biol 5(Suppl):508–512

Guntert P (1998) Structure calculation of biological macromolecules from NMR data. Q Rev Biophys 31(2):145–237

Habenstein B, Wasmer C, Bousset L, Sourigues Y, Schutz A, Loquet A, Meier BH, Melki R, Bockmann A (2011) Extensive de novo solid-state NMR assignments of the 33 kDa C-terminal domain of the Ure2 prion. J Biomol NMR 51(3):235–243. doi:10.1007/s10858-011-9530-4

Habenstein B, Bousset L, Sourigues Y, Kabani M, Loquet A, Meier BH, Melki R, Bockmann A (2012) A native-like conformation for the C-terminal domain of the prion Ure2p within its fibrillar form. Angew Chem Int Ed Engl 51(32):7963–7966

Helmus JJ, Surewicz K, Nadaud PS, Surewicz WK, Jaroniec CP (2008) Molecular conformation and dynamics of the Y145Stop variant of human prion protein in amyloid fibrils. Proc Natl Acad Sci USA 105(17):6284–6289

Higman VA, Flinders J, Hiller M, Jehle S, Markovic S, Fiedler S, van Rossum BJ, Oschkinat H (2009) Assigning large proteins in the solid state: a MAS NMR resonance assignment strategy using selectively and extensively 13C-labelled proteins. J Biomol NMR 44(4):245–260

Hodgkinson P, Emsley L (1999) The accuracy of distance measurements in solid state NMR. J Magn Reson 139:46–59

Hong M (1999) Determination of multiple phi-torsion angles in proteins by selective and extensive 13C labeling and two-dimensional solid-state NMR. J Magn Reson 139:389–401

Hong M, Zhang Y, Hu F (2012a) Membrane protein structure and dynamics from NMR spectroscopy. Annu Rev Phys Chem 63:1–24

Hong M, Fritzsching KJ, Williams JK (2012b) Hydrogen-bonding partner of the proton-conducting histidine in the influenza m2 proton channel revealed from (1)h chemical shifts. J Am Chem Soc 134(36):14753–14755

Hu F, Luo W, Hong M (2010) Mechanisms of proton conduction and gating in influenza M2 proton channels from solid-state NMR. Science 330(6003):505–508

Jehle S, Rajagopal P, Bardiaux B, Markovic S, Kuhne R, Stout JR, Higman VA, Klevit RE, van Rossum B-J, Oschkinat H (2010) Solid-state NMR and SAXS studies provide a structural basis for the activation of alphaB-crystallin oligomers. Nat Struct Mol Biol 17(9):1037–1042

LeMaster DM, Kushlan DM (1996) Dynamical mapping of *E. coli* thioredoxin via 13C NMR relaxation analysis. J Am Chem Soc 118(39):9255–9264

Lewandowski JR, van der Wel PC, Rigney M, Grigorieff N, Griffin RG (2011) Structural complexity of a composite amyloid fibril. J Am Chem Soc 133(37):14686–14698

Lopez del Amo JM, Schmidt M, Fink U, Dasari M, Fandrich M, Reif B (2012) An asymmetric dimer as the basic subunit in Alzheimer's disease amyloid beta fibrils. Angew Chem Int Ed Engl 51(25):6136–6139

Loquet A, Giller K, Becker S, Lange A (2010) Supramolecular interactions probed by 13C–13C solid-state NMR spectroscopy. J Am Chem Soc 132(43):15164–15166

Loquet A, Lv G, Giller K, Becker S, Lange A (2011) (13)C spin dilution for simplified and complete solid-state NMR resonance assignment of insoluble biological assemblies. J Am Chem Soc 133(13):4725–4727

Loquet A, Habenstein B, Demers JP, Becker S, Lange A (2012a) Structure of a bacterial nanomachine: the type 3 secretion system needle. Med Sci (Paris)

Loquet A, Sgourakis NG, Gupta R, Giller K, Riedel D, Goosmann C, Griesinger C, Kolbe M, Baker D, Becker S, Lange A (2012b) Atomic model of the type III secretion system needle. Nature 486(7402):276–279

Lundstrom P, Teilum K, Carstensen T, Bezsonova I, Wiesner S, Hansen DF, Religa TL, Akke M, Kay LE (2007) Fractional 13C enrichment of isolated carbons using [1-13C]- or [2-13C]-glucose facilitates the accurate measurement of dynamics at backbone Calpha and side-chain methyl positions in proteins. J Biomol NMR 38(3):199–212

Lv G, Kumar A, Giller K, Orcellet ML, Riedel D, Fernandez CO, Becker S, Lange A (2012) Structural comparison of mouse and human alpha-synuclein amyloid fibrils by solid-state NMR. J Mol Biol 420(1–2):99–111

Markwick PR, Malliavin T, Nilges M (2008) Structural biology by NMR: structure, dynamics, and interactions. PLoS Comput Biol 4(9):e1000168

McDermott A, Polenova T (2007) Solid state NMR: new tools for insight into enzyme function. Curr Opin Struct Biol 17(5):617–622

Nielsen JT, Bjerring M, Jeppesen MD, Pedersen RO, Pedersen JM, Hein KL, Vosegaard T, Skrydstrup T, Otzen DE, Nielsen NC (2009) Unique identification of supramolecular structures in amyloid fibrils by solid-state NMR spectroscopy. Angew Chem Int Ed Engl 48(12):2118–2121

Pauli J, Baldus M, van Rossum B, de Groot H, Oschkinat H (2001) Backbone and side-chain 13C and 15N signal assignments of the alpha-spectrin SH3 domain by magic angle spinning solid-state NMR at 17.6 Tesla. ChemBioChem 2(4):272–281

Petkova AT, Ishii Y, Balbach JJ, Antzutkin ON, Leapman RD, Delaglio F, Tycko R (2002) A structural model for Alzheimer's beta-amyloid fibrils based on experimental constraints from solid state NMR. Proc Natl Acad Sci USA 99(26):16742–16747

Reif B (2012) Ultra-high resolution in MAS solid-state NMR of perdeuterated proteins: implications for structure and dynamics. J Magn Reson 216:1–12

Renault M, Cukkemane A, Baldus M (2010) Solid-state NMR spectroscopy on complex biomolecules. Angew Chem Int Ed Engl 49(45):8346–8357

Schneider R, Etzkorn M, Giller K, Daebel V, Eisfeld J, Zweckstetter M, Griesinger C, Becker S, Lange A (2010) The native conformation of the human VDAC1N terminus. Angew Chem Int Ed Engl 49:1882–1885

Schuetz A, Wasmer C, Habenstein B, Verel R, Greenwald J, Riek R, Bockmann A, Meier BH (2010) Protocols for the sequential solid-state NMR spectroscopic assignment of a uniformly labeled 25 kDa protein: HET-s(1–227). ChemBioChem 11(11):1543–1551

Shaka AJ, Keeler J, Frenkiel T, Freeman R (1983) An improved sequence for broad-band decoupling—Waltz-16. J Magn Reson 52(2):335–338

Shi L, Ahmed MA, Zhang W, Whited G, Brown LS, Ladizhansky V (2009) Three-dimensional solid-state NMR study of a seven-helical integral membrane proton pump–structural insights. J Mol Biol 386(4):1078–1093

Sperling LJ, Nieuwkoop AJ, Lipton AS, Berthold DA, Rienstra CM (2010) High resolution NMR spectroscopy of nanocrystalline proteins at ultra-high magnetic field. J Biomol NMR 46(2):149–155

Sun S, Han Y, Paramasivam S, Yan S, Siglin AE, Williams JC, Byeon IJ, Ahn J, Gronenborn AM, Polenova T (2012) Solid-state NMR spectroscopy of protein complexes. Methods Mol Biol 831:303–331

Takeuchi K, Gal M, Takahashi H, Shimada I, Wagner G (2011) HNCA-TOCSY-CANH experiments with alternate (13)C–(12)C labeling: a set of 3D experiment with unique supra-sequential information for mainchain resonance assignment. J Biomol NMR 49(1):17–26

Teilum K, Brath U, Lundstrom P, Akke M (2006) Biosynthetic 13C labeling of aromatic side chains in proteins for NMR relaxation measurements. J Am Chem Soc 128(8):2506–2507

Tycko R (2006) Molecular structure of amyloid fibrils: insights from solid-state NMR. Q Rev Biophys 39(1):1–55

Vranken WF, Boucher W, Stevens TJ, Fogh RH, Pajon A, Llinas M, Ulrich EL, Markley JL, Ionides J, Laue ED (2005) The CCPN data model for NMR spectroscopy: development of a software pipeline. Proteins 59(4):687–696

Ward ME, Shi L, Lake E, Krishnamurthy S, Hutchins H, Brown LS, Ladizhansky V (2011) Proton-detected solid-state NMR reveals intramembrane polar networks in a seven-helical transmembrane protein proteorhodopsin. J Am Chem Soc 133(43):17434–17443

Wasmer C, Lange A, Van Melckebeke H, Siemer AB, Riek R, Meier BH (2008) Amyloid fibrils of the HET-s(218–289) prion form a beta solenoid with a triangular hydrophobic core. Science 319(5869):1523–1526

Wüthrich K (1986) NMR of proteins and nucleic acids. Wiley, New York, NY

Yonekura K, Maki-Yonekura S, Namba K (2003) Complete atomic model of the bacterial flagellar filament by electron cryomicroscopy. Nature 424(6949):643–650